ELSEVIER

Polymer 42 (2001) 7429–7441

polymer

www.elsevier.nl/locate/polymer

Synthesis and crystallization behavior of poly(L-lactide)-*block*-poly(ϵ-caprolactone) copolymer

Jin Kon Kim[a,*], Dong-Jin Park[a], Myung-Se Lee[a], Kyo Jin Ihn[b]

[a]*Department of Chemical Engineering and Polymer Research Institute, Electronic and Computer Engineering Divisions, Pohang University of Science and Technology, Pohang, Kyungbuk 790-784, South Korea*

[b]*Department of Chemical Engineering, Kangwon National University, Chunchon 200-701, South Korea*

Received 24 July 2000; received in revised form 5 January 2001; accepted 20 February 2001

Abstract

We investigate, via wide and small angle X-ray scattering methods (WAXS and SAXS), differential scanning calorimetry (DSC), and optical microscopy (OM), the crystallization behavior of poly(L-lactide)-*block*-poly(ϵ-caprolactone) copolymer (PLLA-*b*-PCL) which is classified as a semicrystalline–semicrystalline block copolymer. The synthesis of PLLA-*b*-PCL was done by using a macroinitiator of hydroxy-terminated PCL (PCL-OH) with various molecular weights and followed by ring opening polymerization of L-lactide. The PLLA-*b*-PCL(H) with the number-average molecular weight (M_n) of 77,000 and the weight fraction of PCL block (w_{PCL}) of 0.32 showed microphase-separated structures at molten state up to 220°C, as determined from rheological measurement. But, the PLLA-*b*-PCL(L) with $M_n = 19{,}000$ and $w_{PCL} = 0.374$ became homogeneous at temperatures higher than 175°C.

From the crystallization behavior at 110 and 140°C, we conclude that the chain folding of the crystalline PLLA block in PLLA-*b*-PCL(H) was quite different from that in PLLA-*b*-PCL(L). This result suggests that the chain segregation between the blocks at molten state affected significantly the chain folding of a semicrystalline block during the crystallization. © 2001 Published by Elsevier Science Ltd.

Keywords: Crystallization of block copolymer; Chain folding; Chain segregation

1. Introduction

Poly(L-lactide) (PLLA) has been widely used for many medical purposes, such as suturing and bond fixture because of its excellent biodegradability by hydrolysis [1]. However, the application of PLLA to commercial products like agricultural films is currently still in its infancy. The main reason is its brittleness. This weakness might be improved when a polymer with a lower glass transition temperature is used together. One of the candidates for this purpose is poly(ϵ-caprolactone) (PCL), which is also biodegradable [2]. Due to the lower glass transition temperature of PCL (ca. −50°C), the elongation at the break is very large (≥600%). There are two general approaches to add a PCL to a PLLA: physical blending, or synthesizing PLLA–PCL copolymer. Since a PLLA with a high molecular weight is usually immiscible with PCL even at molten temperatures, the morphology of PLLA/PCL blend becomes coarse and the adhesion strength becomes poor; thus desirable mechanical properties are not anticipated. On the other hand, PLLA-*b*-PCL copolymers have various microdomain structures depending upon the block length ratio between two blocks. The mechanical properties as well as biodegradability are very much affected by the crystallinity of constituent blocks that in turn depends upon the microdomain structures.

During the last decade, much research has been focused on the crystallization behavior of block copolymers with at least one crystallizable block. The block copolymers investigated in the literature are (i) hydrogenated polybutadiene [HPB] based materials [3–15] such as HPB-*b*-poly(ethylene-*ran*-propylene), HPB-*b*-polystyrene [PS], HPB-*b*-poly(ethyl ethylene), HPB-*b*-poly(vinyl cyclohexane), HPB-*b*-poly(head-to-head propylene); (ii) poly(ethylene oxide) [PEO] based materials [16–19] such as PEO-*b*-poly(propylene oxide), PEO-*b*-poly(butylene oxide), PEO-*b*-PS; and (iii) PCL-based materials [20–22] such as PCL-*b*-poly(ethylene glycol) [PEG], PCL-*b*-polybutadiene. Since HPB block was prepared by hydrogenation of poly(1,4-butadiene) [PB] made from an anionic polymerization, 1,2 addition in the PB always exists. This portion becomes the ethyl branch in HPB (2–3 ethyl branches per 100 carbons); thus T_m of HPB (l00–110°C) is lower than that (~140°C) of

* Corresponding author. Tel.: +82-54-279-2276; fax: +82-54-279-8298.
E-mail address: jkkim@postech.ac.kr (J.K. Kim).

0032-3861/01/$ - see front matter © 2001 Published by Elsevier Science Ltd.
PII: S0032-3861(01)00217-8

a high-density polyethylene (HDPE) commercially available. The branch density becomes more important than the thermodynamic parameter such as the degree of supercooling [8]. On the other hand, since there is no branch in PEO chain, the length of folded chain of the PEO block was mainly affected by the quenching depth and annealing time. The T_m of PEO block in a block copolymer is lower than that of PEO homopolymer [18]. The number of folds is influenced by the existence of amorphous block chains. For PCL–PEG where two blocks are crystallized, the crystallinity of one block becomes zero when this block is less than 25 wt%, while the crystallinity of one component in the PCL–PEG blend is not equal to zero even when this component is less than 25 wt% [21].

One of the most important issues in a crystallizable block copolymer is to find the chain (or lamellar) folding [4,8,11,23]. The chain folding of the crystallizable block in amorphous–crystalline block copolymers depends upon the segregation of two blocks in the molten state. For instance, when block copolymers are homogeneous or weak segregation in the molten state, the chain folding becomes a 'perpendicular folding' where the chain folding is perpendicular to the lamellar layer. On the other hand, when block copolymers are strong segregation (or well-defined microdomain structures) in the molten state, the chain folding becomes 'parallel folding' where the chain folding is parallel to the lamellar layer [23]. However, the chain folding mechanism of a block copolymer during the crystallization has not been investigated in detail.

In this study, we investigated, using small-angle and wide-angle X-ray scattering (SAXS and WAXS), differential scanning calorimetry (DSC), and optical microscopy (OM), crystallization behavior and the chain folding orientation of PLLA block in PLLA-*b*-PCL copolymers. Emphasis was placed on the effect of the segregation degree at molten state (or the total molecular weight of block copolymer) on crystallization behavior of PLLA block. Even though both blocks in PLLA-*b*-PCL copolymers were crystallized at lower temperatures, we only considered the crystallization behavior of PLLA block. This is done when the crystallization occurs at specific temperatures between the T_ms of PLLA and PCL (namely $65°C < T_c < 175°C$). We report on the highlights of our findings.

2. Experimental

2.1. Synthesis and characterization

We synthesized PLLA-*b*-PCL copolymers using the macroinitiator according to Scheme 1 [24]. First, hydroxy-terminated PCL (PCL-OH) with various molecular weights was prepared by changing the molar ratio of ϵ-caprolactone (CL: Aldrich Chem. Co) to dodecanol (Aldrich Chem. Co.) in the presence of stannous octoate (Aldrich Chem. Co.) at 140°C for 24 h. The degree of polymerization of PCL-OH was determined, via ^{1}H nuclear magnetic resonance spectroscopy (NMR, Brucker DRX500), from the area ratio of the peak at $\delta = 4.05$ ppm corresponding to the ethylene hydrogen attached to the oxygen in a repeating CL unit to that at $\delta = 3.65$ ppm corresponding to the ethylene hydrogen attached to the end OH group. Then, PLLA-*b*-PCL copolymers were synthesized by ring-opening polymerization of L-lactide (LLA: Aldrich Chem. Co.) initiated by PCL-OH in the presence of stannous octoate at 110°C for

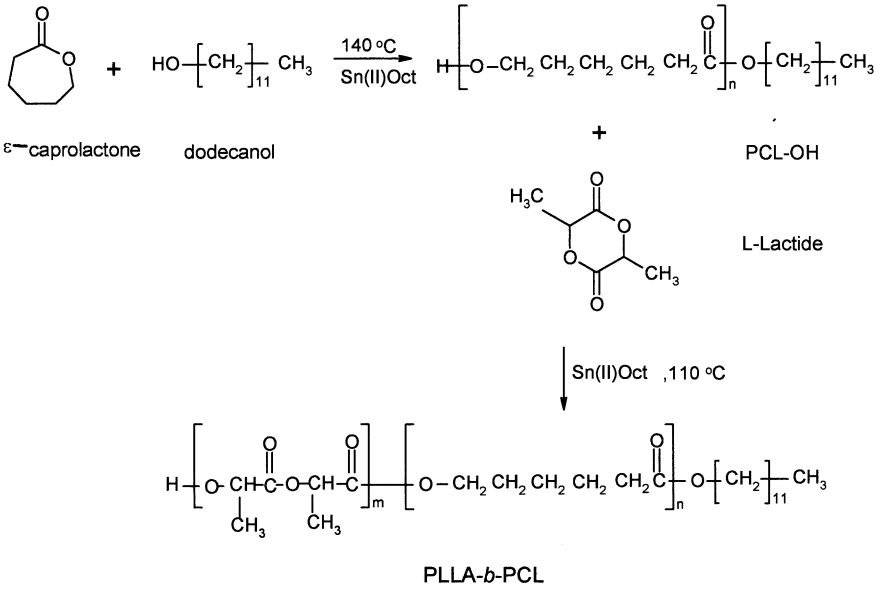

Scheme 1.

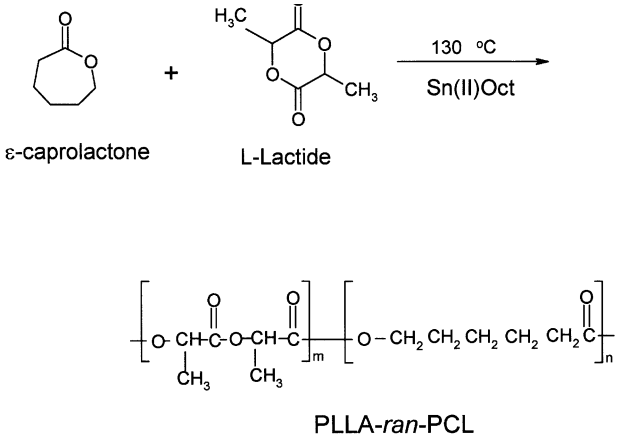

Scheme 2.

48 h. A PLLA–PCL random copolymer (PLLA-*r*-PCL) was also prepared according to Scheme 2 by simultaneous addition of two monomers (LLA and CL) into a reactor in the presence of stannous octoate at 130°C for 48 h [25]. After the reaction, copolymers were first dissolved into chloroform and then precipitated by using nonsolvent (the mixture of acetone and *n*-hexane (40:60 v/v)). Finally, the products were vacuum-dried at room temperature for 3 weeks. The mole fraction of PCL in the block and random copolymers were determined, via ^{1}H NMR, from the area of the peak at $\delta = 4.05$ ppm divided by the sum of the area of the peak at $\delta = 4.05$ ppm and the area of the peak at $\delta = 5.15$ ppm corresponding to methine hydrogen in $-[OCH(CH_3)]$. Gel permeation chromatography (GPC; Waters 600E, Millipore) with tetrahydrofuran as a solvent and a solid content of 0.2 wt% was employed to determine the molecular weight and the distribution of the PLLA-*b*-PCLs, PLLA-*r*-PCL, and neat PLLA and PCL. All molecular weights were determined by using a calibration curve prepared with PS standards. Molecular characterization of all block copolymers and a random copolymer as well as neat PLLA and PCL is given in Table 1.

Table 1
Molecular characterization of polymers employed in this study

	M_n [a]	Wt% [a] (PCL)	Volume fraction of PCL at 190°C	M_n [b]	M_w/M_n [b]
PLLA-*ran*-PCL	–	32.2	0.38	64,000	1.6
PLLA-*b*-PCL(HH)	160,000	13.7	0.18	141,000	1.4
PLLA-*b*-PCL(H)	77,000	32.2	0.38	97,000	1.56
PLLA-*b*-PCL(M)	46,000	54.0	0.59	61,000	1.30
PLLA-*b*-PCL(L)	19,000	37.4	0.42	21,000	1.41
PLLA	–	0	0	153,000	1.59
PCL	–	100	1.0	100,000	1.38

[a] Determined by ^{1}H NMR.
[b] Determined by GPC with PS standards.

2.2. Calorimetric measurements

The melting point (T_m) and the melting endotherm (ΔH_m) of the PLLA and PCL blocks in the block copolymers and the random copolymers as well as those of neat PLLA homopolymer were measured by differential scanning calorimetry (DSC, Perkin–Elmer DSC 7 series). Prior to measurement, the baseline was established by using two empty pans. To prevent thermal degradation, nitrogen gas was circulated around the sample pan. Each sample of about 10 mg was heated at a heating rate of 10°C/min from 25 to 190°C. DSC thermograms of all samples were obtained from the first heating run if further temperature histories were not given.

The isothermal crystallization of the PLLA block in PLLA-*b*-PCLs was carried out at two temperatures (140 and 110°C) after a specimen was annealed for 5 min at 190°C and followed by quenching in a DSC sample pan.

2.3. Optical microscopy

The crystallization kinetics and spherulite sizes of the PLLA block in the PLLA-*b*-PCLs were measured with an optical microscope (Axioplan, Zeiss Co.). Fresh nitrogen gas was circulated into the heating block attached to the optical microscope to avoid any thermal oxidative degradation. The specimen was prepared by direct pressing of each blend in the molten state without using a spacer, and the thickness was ~15 μm. The morphology of a specimen after crystallization was also investigated by using a polarized mode in the microscope when temperature was decreased from 190°C to two crystallization temperatures (140 and 110°C).

2.4. Small and wide angle X-ray scattering

SAXS measurements with synchrotron radiation were conducted at the 3C2 and 1B2 beam lines at the Pohang Light Source (PLS), Korea [26]. The primary beam was monochromatized with double Si (111) crystals at a wavelength of 0.15402 nm (the photon energy of X-ray is 7.76 keV) and then it was focused on a detector plane by a bent cylindrical mirror. A one-dimensional position-sensitive detector (Diode-Array PSD; Princeton Instruments Inc.; Model ST-120) with the distance of each diode of 25 μm was used. We subtracted the scattering intensity of an empty cell with two pieces of thin polyimide (Kapton) films from that of samples by taking into account the transmittance of X-rays through the samples. The contribution of thermal diffuse scattering (TDS) arising from the density fluctuations was further subtracted. Here, we approximated that the intensity at higher q region, where the scattering intensity is independent of q, is identical to the intensity level of TDS. Here, q is the magnitude of the scattering vector, $q = (4\pi/\lambda)\sin(\theta/2)$, where λ and θ are the wavelength of the X-rays and the scattering angle, respectively.

The obtained scattering intensities were not converted to the absolute unit. The PLLA block in the PLLA-*b*-PCLs and the homopolymer of PLLA with the thickness of 1 mm were crystallized at 140 and 110°C after a specimen was quenched from 190°C. Then, SAXS profiles during the isothermal crystallization at two temperatures were measured at every minute up to 2 h. The exposure time was 30 s.

The WAXS measurements were also conducted at the 3C2 and 1B2 beam lines at the Pohang Light Source (PLS), Korea after the specimen was quenched from 190°C to either 140 or 110°C. The exposure time was 1 min. In this situation, a 2D CCD camera (Princeton Instruments Inc.; SCX-TE/CCD-1242E) was used because we easily determined the intensities up to smaller angles ($2\theta \sim 5°$). Since all scatterings showed ring patterns, the scattering intensity at a given q was obtained from the circular average of 2D intensity.

3. Results and discussion

3.1. Microdomain structures at molten states

Fig. 1 gives DSC thermograms obtained during the first heating run at a rate of 10°C/min for PLLA-*b*-PCL(H), PLLA-*b*-PCL(L), PLLA-*r*-PCL, and neat PLLA and PCL. The block copolymers have two T_ms at 175 and 65°C corresponding to the T_ms of the PLLA block and the PCL block, while a random copolymer has a single T_m at 135°C. The T_m of PLLA block in PLLA-*b*-PCL(L) is lower than that of neat PLLA and the PLLA block in PLLA-*b*-PCL(H) because of a lower molecular weight of PLLA block (10,000). Neat PLLA also has a glass transition temperature (T_g) near 67°C.

In order to determine the microdomain structures of PLLA-*b*-PCL(H) and PLLA-*b*-PCL(L) at molten state, we tried to measure SAXS profiles at temperatures between 180 and 220°C. However, due to a very small electron density difference between the PLLA and the PCL blocks at molten state, any peak corresponding either to a microdomain or to a concentration fluctuation resulting from the correlation hole effect was not observed in SAXS profiles. But we could indirectly determine the order-to-disorder transition temperature (T_{ODT}) of PLLA-*b*-PCLs by using a rheological criterion of logarithmic plots of storage modulus (G') versus loss modulus (G'') [27–31]. These plots become temperature-independent at temperatures larger than the T_{ODT} of a block copolymer. Fig. 2(a) gives log G' versus log G'' plots for PLLA-*b*-PCL(H) and PLLA-*b*-PCL(L) at various temperatures. It is seen that the PLLA-*b*-PCL(H) showed temperature-dependence up to 220°C, above which the degradation of the PLLA block might occur. Also, the slope in this plot is much smaller than 2; thus, the PLLA-*b*-PCL(H) has microphase-separated structures up to 220°C. On the other hand, the PLLA-*b*-PCL(L) became homogeneous at temperatures higher than 175°C due to lower molecular weight. Of course, log G' versus log G'' plots for a neat PLLA and a PLLA-*r*-PCL become independent of temperature as shown in Fig. 2(b).

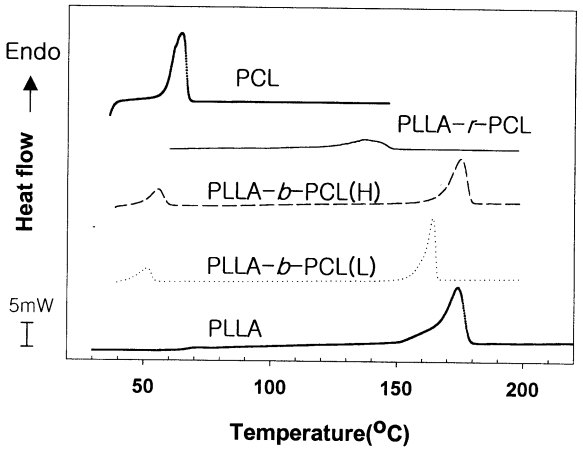

Fig. 1. DSC thermograms of PLLA-*b*-PCL(H), PLLA-b-PCL(L), PLLA-*r*-PCL, and neat PCL and PLLA.

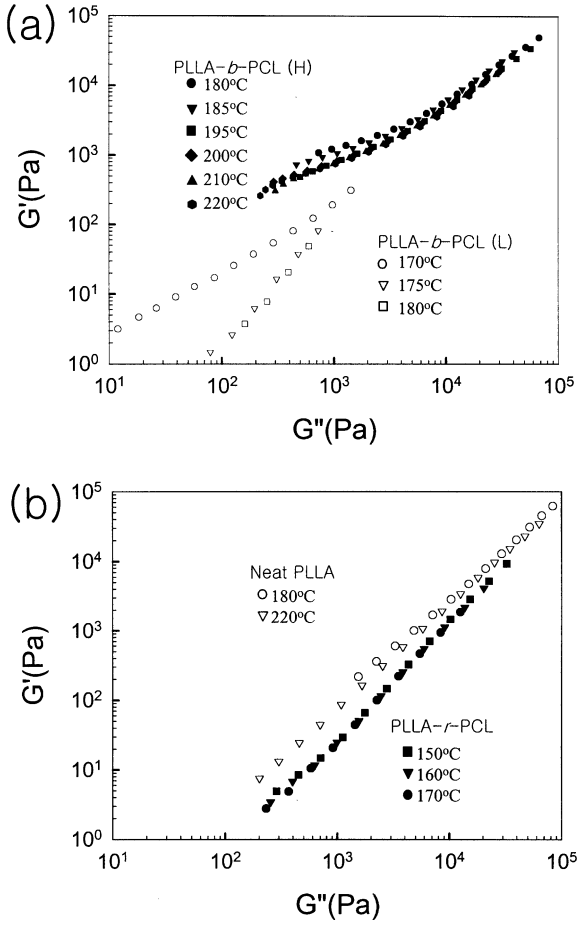

Fig. 2. Log G' versus log G'' at various temperatures: (a) two PLLA-*b*-PCLs: filled symbols for PLLA-*b*-PCL(H), open symbols for PLLA-*b*-PCL(L); (b) PLLA-*r*-PCL and neat PLLA: filled symbols for PLLA-*r*-PCL, open symbols for neat PLLA.

Even though the microdomain structure of PLLA-*b*-PCL(H) is not exactly determined due to the absence of the SAXS peak, the most probable microdomains of this block copolymer at molten state are lamellar microdomain. This is judged from the information of the volume fraction of the PCL block (0.38) at molten state. Here, the densities of PLLA and PCL to calculate the volume fraction are 1.24 [32] and 1.02 g/cm^3 [33] at 190°C, respectively. The microdomain of PLLA-*b*-PCL copolymers would be determined by using a small-angle neutron scattering method after one block is deuterated.

3.2. Crystallization behavior of PLLA-block-PCL(H)

Fig. 3 gives the change of the heat flow with isothermal crystallization time at 140 and 110°C for PLLA-*b*-PCL(H) after a specimen was quenched from 190°C. Only PLLA block can crystallize at these two temperatures since the T_m of PCL was 65°C. The crystallization at 110°C finished within 14 min, while that at 140°C continued up to 2 h. It is generally known that the fast crystallization occurs at mid point (~122°C) between T_g and T_m. Thus, the slow crystallization at 140°C compared with that at 110°C is due to the dominant effect of the thermodynamic driving force of crystallization (or quenching depth) compared with the kinetics (or mobility) of the chains. From Fig. 3, we calculated the relative crystallinity at each time, $\phi_c(t)$, defined by

$$\phi_c(t) = \Delta H_c(t)/\Delta H_c(t = \infty) \quad (1)$$

where $\Delta H_c(t)$ is the heat of crystallization at time t, which was determined by the exothermic area up to time t. The relative crystallinity can be described by the Avrami equation:

$$\phi_c(t) = 1 - \exp(-kt^n) \quad (2)$$

where k is the rate constant and n is the Avrami's exponent. From the Avrami plot for PLLA-*b*-PCL(H) (Fig. 4), the values of n for both 140 and 110°C were determined to be

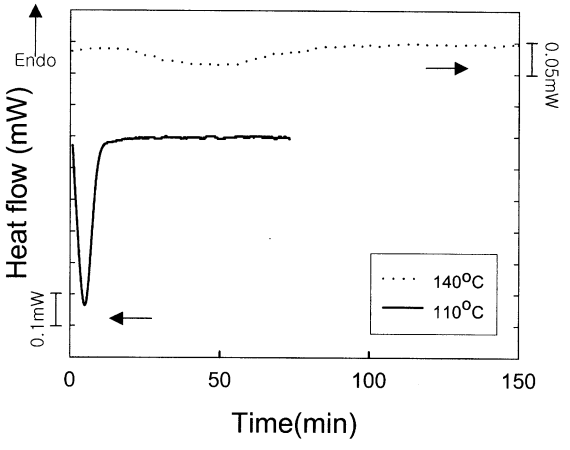

Fig. 3. Heat flow change during the crystallization at 110 and 140°C for PLLA-*b*-PCL(H) after quenching from 190°C.

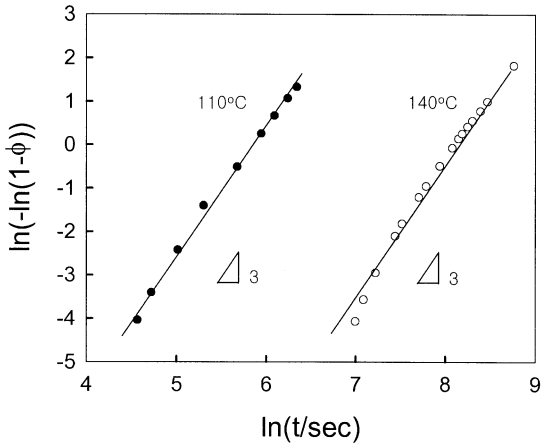

Fig. 4. Avrami plot at 110 and 140°C for the PLLA-*b*-PCL (H).

3.0 ± 0.15. We found that the half times ($t_{1/2}$) at 140 and 110°C were 50.8 and 5.2 min, respectively. OM images for PLLA-*b*-PCL(H) at 140 and 110°C were shown in Figs. 5 and 6, respectively, from which the spherulites are seen during the entire crystallization process. Of course, the spherulite size at 140°C is much larger than that at 110°C because of the smaller quenching depth. We also found that the time for spherulites to fill the entire volume as shown in Fig. 5 is almost the same as the time for the complete crystallization as shown in the DSC thermogram (see Fig. 3). Thus, the increase in the crystallinity of PLLA block with time is mainly due to the increase in the degree of filling of the spherulite. This implies that the intraspherulitic (secondary) crystallization contributes little to the development of crystallinity measured by DSC.

In order to determine the crystallinity of PLLA block with crystallization time at 140 and 110°C, a specimen was annealed at 190°C for 5 min followed by quenching to two temperatures (140 and 110°C). After being crystallized

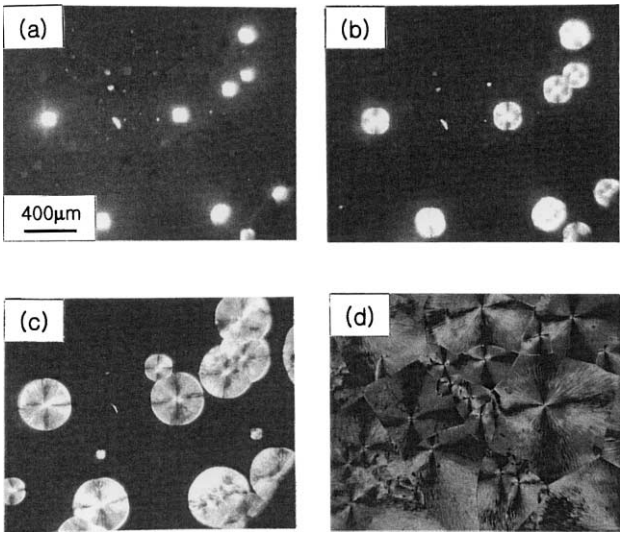

Fig. 5. OM micrographs for PLLA-*b*-PCL(H) at 140°C for various crystallization times (min): (a)15; (b)30; (c)60; (d)120.

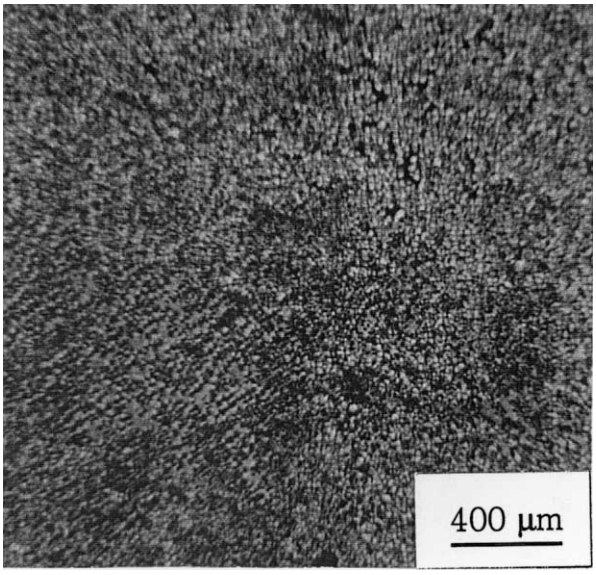

Fig. 6. OM micrograph of PLLA-*b*-PCL(H) crystallized at 110°C for 4 min after quenching from 190°C.

for various times, a specimen was heated to 200°C at a heating rate of 10°C/min. The degree of the crystallinity was obtained:

$$X_c(t) = \Delta H_m(t)/(w_{PLLA}\Delta H_{m,0}) \quad (3)$$

where $\Delta H_m(t)$ is the area of the melting endotherm of PLLA block at time t, w_{PLLA} is the weight fraction of the PLLA block in the PLLA-*b*-PCL(H), and $\Delta H_{m,0}$ is the melting endotherm (93.7 J/g) at equilibrium [34]. The change in $X_c(t)$ with time is shown in Fig. 7, from which we note that the $X_c(t)$ at 140°C reaches a saturation at $t > 2$ h, while that at 110°C reaches a saturation at $t = 15$ min. Interestingly, even though the crystallization at 110°C occurs faster than that at 140°C, the final crystallinity at 140°C is higher than that at 110°C. This is due to the difference in lamellar thickness in crystalline phase and/or domain spacing of the spherulites.

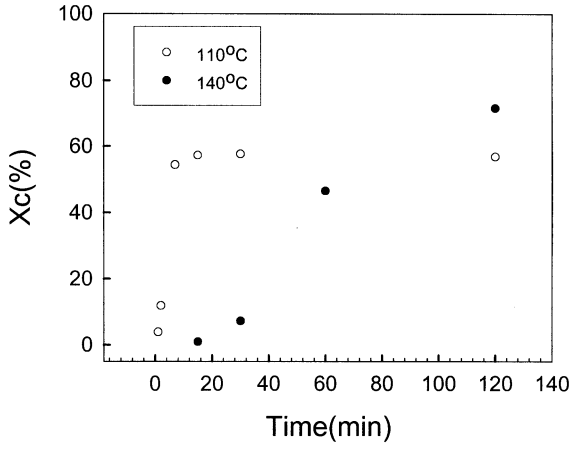

Fig. 7. Crystallinity change with time determined by DSC at 110 and 140°C for PLLA-*b*-PCL(H) after quenching from 190°C.

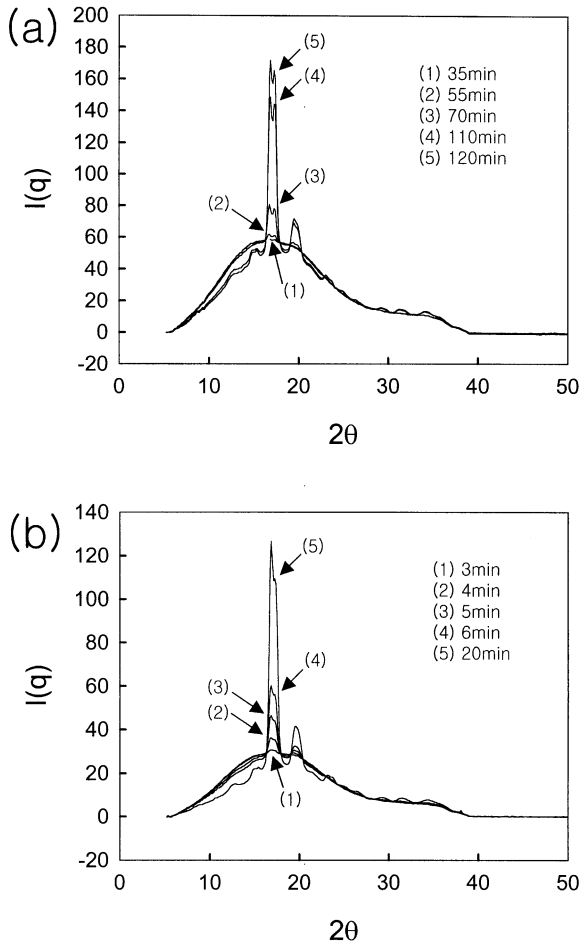

Fig. 8. Plots of WAXS profiles versus scattering angle (2θ) for PLLA-*b*-PCL(H) at various crystallization times at two temperatures: (a) 140°C; (b) 110°C.

Fig. 8 gives WAXS profiles at 140 and 110°C after the specimen was quenched from 190°C. For crystallization at 140°C the peaks at $2\theta = 17$ and 19° (or $q = 6$ and 7 nm^{-1}) corresponding to the crystalline PLLA [35] did not appear until 50 min; thus perfect crystalline regions did not form until this time. With increasing crystallization time, the peak intensities increased and slowly approached a steady value at longer times (say $t > 120$ min. For the crystallization at 110°C, similar behaviors are observed except that the crystallization was completed at earlier times (say less than 20 min). From the results given in Fig. 8, we can obtain the crystallinity of PLLA block at a given crystallization time:

$$X_c(t) = I_c(t)/[w_{PLLA}(I_c(t) + I_a(t))] \quad (4)$$

where $I_c(t)$ and $I_a(t)$ are the crystalline and amorphous areas that were obtained from the peak separation. It is seen in Fig. 9 that the crystallinity obtained from WAXS was qualitatively in agreement with DSC results (see Fig. 7). The small crystallinity at a given time obtained from WAXS compared with DSC results is because only appropriate

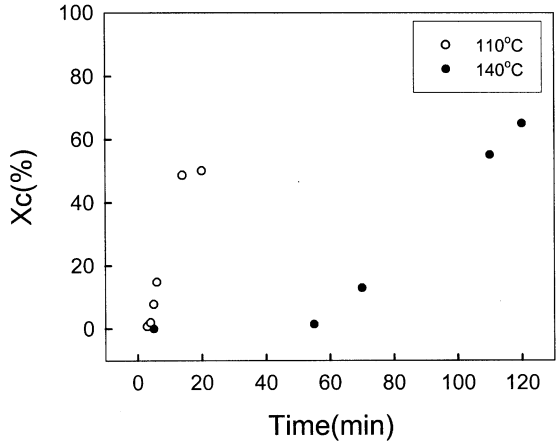

Fig. 9. Crystallinity change with time determined by WAXS at 110 and 140°C for PLLA-*b*-PCL(H) after quenching from 190°C.

crystal size and perfect crystalline region contribute to the crystalline peaks in WAXS.

Now, we consider the long spacing of PLLA-*b*-PCL(H) measured by SAXS. Fig. 10 gives Lorentz-corrected SAXS profiles ($I(q)q^2$ versus q) with crystallization time at 140 and 110°C after a specimen was quenched from 190°C. SAXS intensity near $q = 0.3\ \mathrm{nm}^{-1}$, which resulted from the electron density difference between the crystalline part of the PLLA block and the amorphous part consisting of amorphous PLLA block and PCL block, was increased until the crystallization was completed (see Figs. 3 and 8(a)). The absence of higher order peaks ($2q^*$, $3q^*$, etc.) corresponding to lamellar superstructure might be due to the polydispersity effect. Interestingly, the SAXS intensities at low q (for instance, $\sim 0.12\ \mathrm{nm}^{-1}$) are larger. On the other hand, we found that SAXS intensities at low q are very small for neat PLLA, as shown in Fig. 11. Although the reason for showing higher SAXS intensities at low q is not clear, this might be attributed to the existence of the microdomain structure with alternating lamellar layers consisting of incomplete crystalline PLLA regions, that is, the regions where the PLLA chains are not fully registered in the crystal lattice, plus amorphous regions in PLLA block and amorphous PCL block. As discussed earlier, the microdomain of this block copolymer was not detected in SAXS profile at molten state due to smaller electron density. But, if incomplete crystalline PLLA regions were formed during earlier stage of the crystallization within the PLLA microdomain, those might give the electron density difference from amorphous PCL block. However, we could not see a peak corresponding to the microdomain spacing of the PLLA-*b*-PCL(H) in SAXS profiles. This might be due to a large microdomain spacing of the PLLA-*b*-PCL(H), which corresponds to q^* having less than $\sim 0.08\ \mathrm{nm}^{-1}$. Since the low q-limit of the SAXS device was $\sim 0.1\ \mathrm{nm}^{-1}$, one cannot see a peak when the peak position is less than $0.1\ \mathrm{nm}^{-1}$. Thus, in this situation, SAXS intensity increased simply with decreasing q at low

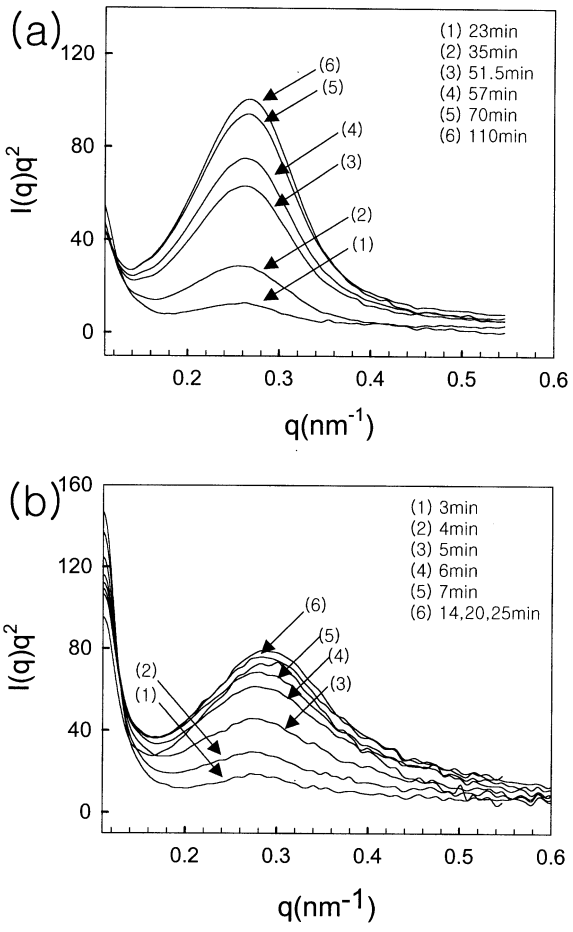

Fig. 10. Lorentz-corrected SAXS intensity versus q for PLLA-*b*-PCL(H) at various crystallization times at two temperatures: (a) 140°C; (b) 110°C.

q regions. This argument will be corroborated later by showing that PLLA-*b*-PCL(L) exhibited clearly this kind of peak.

The main peak in SAXS profiles was due to the

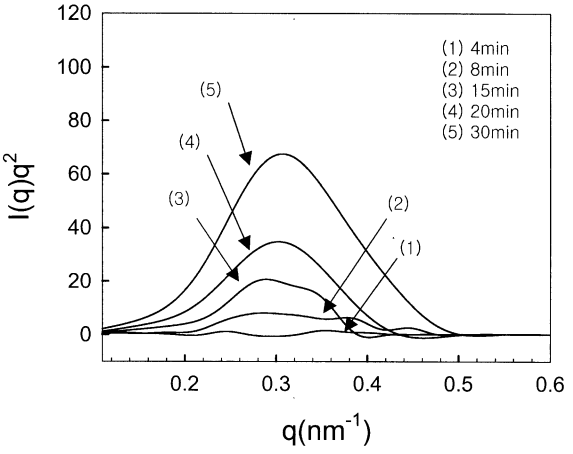

Fig. 11. Lorentz-corrected SAXS intensity versus q for PLLA homopolymer crystallized at 140°C after the specimen was quenched from 190°C.

crystallization of PLLA block with a regular lamellar folding. It is seen in Fig. 10 that the long period d ($=2\pi/q^*$, where q^* is the peak position) at both temperatures slightly decreased with crystallization time. Here, d represents the total lamellar spacing consisting of crystalline and amorphous phases. This implies that d decreased with increasing amount of spherulites. This was attributed to the densification, which might result from the lamellar insertion within the loosely stacked lamellar, with increasing crystallization time, as commonly found in neat homopolymer crystallization [36] (for instance, neat PLLA crystallization as shown in Fig. 11). Also, we found that the peak width as well as the invariant (Q) of SAXS profiles increased with crystallization time. Here, Q is defined by [37]:

$$Q = \int_0^\infty I(q)q^2\,\mathrm{d}q = \phi_s\phi_c(1-\phi_c)(\rho_a-\rho_c)^2 \tag{5}$$

where ϕ_s is the volume fraction of lamellar stacks in the sample, ϕ_c is the volume fraction of crystalline PLLA block in the lamellae, ρ_c and ρ_a are the densities of crystalline and amorphous phases in the lamellae. The increased Q with crystallization time even for $\phi_c > 0.5$ might be due to the increase in ϕ_s.

Now, we consider the thickness of the crystalline PLLA block (L_c) in the lamellae obtained from the one-dimension correlation function $\gamma(z)$ [37]:

$$\gamma(z) = \int_0^\infty I(q)q^2\cos(qz)\,\mathrm{d}q/Q \tag{6}$$

The first maximum in $\gamma(z)$ corresponds to the d, and L_c was determined as shown in Fig. 12 at two different temperatures and complete crystallization. It is known that when a crystallinity of a specimen is less than 50%, the L given in Fig. 12 becomes L_c. Although the crystallinity of neat PLLA is larger than 50%, which was recently reported by Chen et al. [38] as well measured by WAXS and DSC [39], the crystallinity of the PLLA block in the PLLA–PCL block is less than 50% because of the existence of the amorphous PCL block. Thus, the L given in Fig. 12 represents L_c of the PLLA block. From Fig. 12, L_c and d at 140°C are calculated to be 8.2 and 23.1 nm, respectively, while those at 110°C are 6.6 and 21.3 nm, respectively. The larger L_c at higher temperatures is because the L_c is increased with decreasing the degree of the supercooling ($T_m - T_c$) [23].

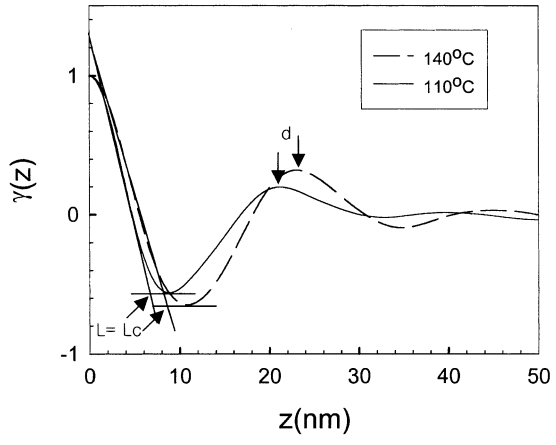

Fig. 12. One-dimensional correlation function of SAXS profiles for PLLA-*b*-PCL(H) crystallized at 140°C for 110 min and 110°C for 25 min.

On the other hand, from Fig. 11 and Eq. (6), L_c and d for neat PLLA at 140°C were calculated to be 12.5 and 21.2 nm, and those at 110°C are 12.3 and 20.8 nm, respectively. Those values of neat PLLA are consistent with recent results for neat PLLA [38]. Of course, in neat PLLA, the length L defined in Fig. 12 became L_a. Interestingly, the d of PLLA-*b*-PCL(H) was just 2 nm larger than that of neat PLLA. But from the volume fraction of the PCL block (ϕ_{PCL}) having 0.38 for the PLLA-*b*-PCL(H), the amorphous PCL block domain might become at least 7 nm ($d \times \phi_{PCL}$).

Thus, we speculate that the chain folding of the PLLA block in PLLA-*b*-PCL(H) might be different from that of neat PLLA. Since neat PLLA has perpendicular lamellar folding, we tentatively considered that the chain folding of the PLLA block in PLLA-*b*-PCL(H) is parallel. Two types of chain folding for a block copolymer have been reported in the literature: perpendicular and parallel chain folding, as shown in Fig. 13. For the perpendicular chain folding, in order to increase the crystalline layer thickness with

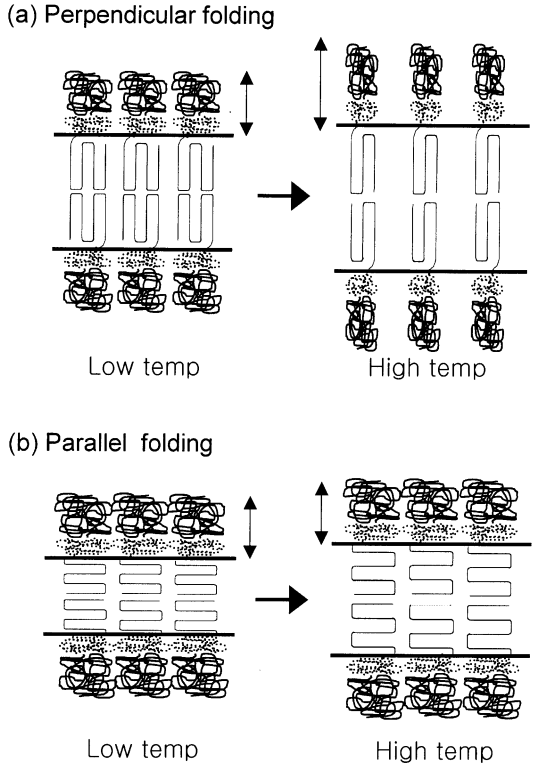

Fig. 13. Domain spacing change depending upon chain folding orientation.

increasing crystallization temperature, the number of chain folding decreases; thus, the area occupied by one crystalline chain decreased. Similarly, the amorphous chain connected to the crystallizable block should have a smaller area, which implies that the amorphous chain should be extended. In this situation, the increase in d is due to the sum of the increase in the crystalline part as well as the increase in the amorphous part. However, for parallel chain folding, the increase in crystalline layer thickness upon heating was due to either the increase in the number of the chain folding at the constant gap of two adjacent chains oriented parallel to the layer or the increase of the gap of two adjacent chains at constant number of chain folding. Among these two, the latter effect would be more important because the free energy penalty to increase the folding number with increasing temperature might be larger. But the area occupied by one crystalline chain does not need to increase; thus, the amorphous length does not increase accordingly.

From Fig. 12, we found that the increase in L_c from 110 to 140°C for the PLLA-*b*-PCL(H) was 1.6 nm, which is very similar to the increase in d (1.8 nm). Thus, we might conclude that the chain folding of the crystalline PLLA block in the PLLA-*b*-PCL(H) at two crystallization temperatures would be parallel orientations. This is consistent with reports that when PE–PEE, PE–PEP, and PE–PVCH block copolymers with strong segregation in molten state are crystallized, the most probable lamellar orientations are parallel [7,11,23]. However, it is not completely excluded that the chain folding of crystalline PLLA block in PLLA-*b*-PCL(H) might not have parallel orientation because spherulite structure was clearly observed after crystallization, as shown in Figs. 5 and 6. Furthermore, PLLA-*b*-PCL(H) has another microdomain structure (for instance, hexagonally packed cylindrical microdomains (HPC)) at molten state; thus the different behavior of the change in L_c and d with temperature between the PLLA-*b*-PCL(H) and neat PLLA might not be only due to the different chain folding, since a block copolymer with the volume fraction of one block with 0.38 might have either lamellar or HPC microdomains at molten state. This possibility is under investigation using a symmetric block copolymer. But, we found that the PLLA-*b*-PCL(M) with M_n of 46,000 and $w_{PLLA} = 0.54$ exhibited perpendicular folding [39]. This block copolymer has the T_{ODT} of 220°C [39], which was not far from the annealing temperature (190°C) before the crystallization; thus this block copolymer is regarded as a weak segregation at 190°C. On the basis of the above argument, we consider that the folding of crystalline PLLA would be parallel.

3.3. Crystallization behavior of PLLA-block-PCL(L)

After measuring heat flow change with isothermal crystallization time at 140 and 110°C after quenching from 190°C, we found that the crystallization was completed within 10 min at 110°C, while that completed after 110 min at 140°C. The half crystallization times at 140 and 110°C were 32.3 and 2.64 min, respectively. The values of n for both 140 and 110°C were determined to be 4.0 ± 0.15. Also, the growth mechanism was spherulite growth, as determined by OM images, as shown in Fig. 14. The exponent for PLLA-*b*-PCL(L) was different from that for PLLA-*b*-PCL(H). This is because the crystallization might mainly occur uniformly for PLLA-*b*-PCL(L).

WAXS profiles during the crystallization of PLLA-*b*-PCL(L) at 140 and 110°C are given in Fig. 15, from which one notes that these are very similar to those of PLLA-*b*-PCL(H) except fast crystallization. It is seen that the $X_c(t)$ at 140°C reaches a steady-state after 2 h, while that at 110°C reaches after 15 min. Interestingly, even though the crystallization at 110°C occurs faster than that at 140°C, the final crystallinity 140°C is higher than that at 110°C, which was a similar phenomenon for PLLA-*b*-PCL(H). Fig. 6 gives Lorentz-corrected SAXS profiles at various crystallization times at 140 and 110°C after a specimen was quenched from 190°C. The SAXS intensity at the main peak ($q^* \sim 0.3\ nm^{-1}$) at 140°C was not observed until $t = 20$ min, then SAXS intensity increased sharply, and finally reached a steady value when the crystallization finished. The d ($=2\pi/q^*$) at two temperatures decreased with increasing crystallization time because of the densification. Very interestingly, these SAXS profiles are different from those for PLLA-*b*-PCL(H) (see Fig. 10) since another peak near $q \sim 0.2\ nm^{-1}$ was clearly observed for PLLA-*b*-PCL(L) at shorter times. Of course, with increasing time, this peak intensity decreased and finally this peak disappeared. After a complete disappearance of this peak, a main peak near $q^* \sim 0.3\ nm^{-1}$ was observed. Thus, we do not consider that the peak at $q \sim 0.2\ nm^{-1}$ corresponds to the equilibrium properties, namely, the domain spacing of the crystalline part of PLLA block with complete lamellar ordering and the amorphous part. Rather, it was due to the

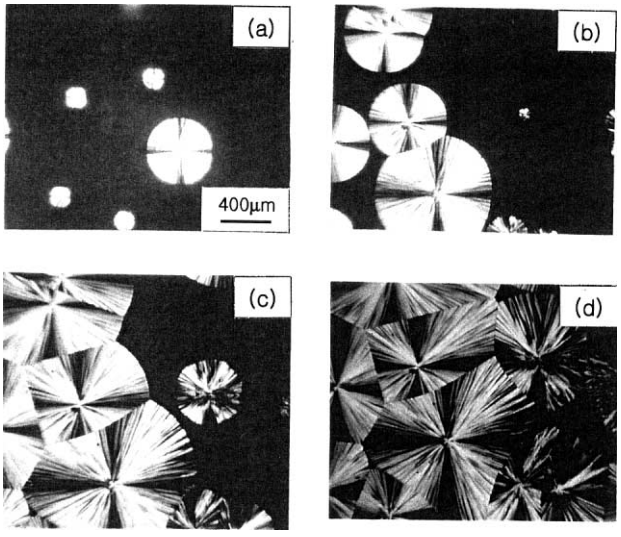

Fig. 14. OM micrographs for PLLA-*b*-PCL(L) at 140°C for various crystallization times (min): (a) 15; (b) 30; (c) 60; (d) 120.

existence of the microdomain structure with alternating lamellar layers consisting of incomplete crystalline plus amorphous parts in PLLA block and amorphous PCL block. However, at this stage, complete crystallization of PLLA did not occur, because there was no PLLA crystalline peaks in WAXS profiles (see Fig. 15) as long as the peak at $q \sim 0.2\ \mathrm{nm}^{-1}$ was observed. The existence of the similar microdomain structure was also found for PLLA-*b*-PCL(M) having the molecular weight (M) of 46,000. This block exhibited clearly a peak at $q \sim 0.12\ \mathrm{nm}^{-1}$ before a main SAXS peak at $q = 0.19\ \mathrm{nm}^{-1}$ appeared [39]. If a peak resulted from earlier stage of crystallization process corresponds to the microdomain spacing (D), D is proportional to the two-third power of M [40]. Then, the value of D for the PLLA-*b*-PCL(M) is predicted to be 1.80 times large than that for the PLLA-*b*-PCL(L), which is close to experimental results (1.7). If this concept is also applicable to the PLLA-*b*-PCL(H), the peak corresponding to D would be observed at $\sim 0.08\ \mathrm{nm}^{-1}$, which is outside the low q-limit of the SAXS device. Thus, larger SAXS intensity at $q \sim 0.1\ \mathrm{nm}^{-1}$ for the PLLA-*b*-PCL(H), as shown in Fig. 10, might also be attributed to the existence of the microdomain structure. Since the crystallization proceeds at the expense of the microdomain structure, the peak intensity at $q \sim 0.2\ \mathrm{nm}^{-1}$ for the PLLA-*b*-PCL(L) decreases, whereas the peak intensity at $q \sim 0.3\ \mathrm{nm}^{-1}$ increased with crystallization time (Fig. 16).

On the basis of these results, the mechanism of the crystallization of PLLA-*b*-PCL(L) can be speculated on as shown in Fig. 17. During earlier times of crystallization, two blocks might experience microphase-separation driven by the crystallization driving force of the PLLA block, and the microdomain structure with alternating lamellar layer would be developed. These PLLA chains have different electron density from the amorphous PLLA chains existing at higher temperatures. Thus, SAXS scattering occur due to the contrast between these chains and amorphous PCL chains, as shown in Fig. 17(b). In this situation, the d might represent the domain spacing. But, due to the absence of WAXS peaks near $2\theta = 17$ and 19°, the crystallization with regular chain folding does not occur at this stage. With further increase in crystallization, microphase-separation is totally destroyed. And, all PLLA chains have regular lamellar foldings; thus in this situation the d corresponds exactly to the crystalline lamellar distance, as given in Fig. 17(c).

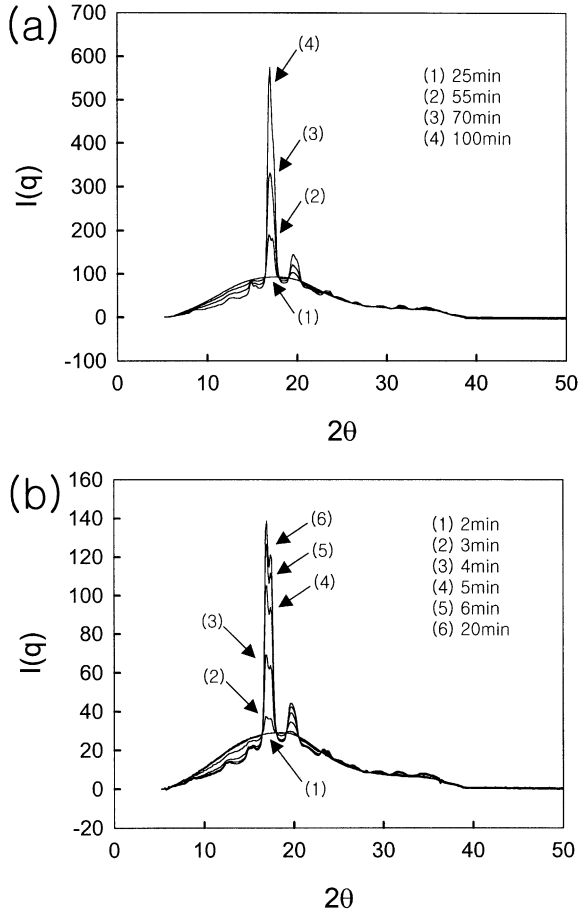

Fig. 15. Plots of WAXS profiles versus scattering angle (2θ) for PLLA-*b*-PCL(L) at various crystallization times at two temperatures: (a) 140°C; (b) 110°C.

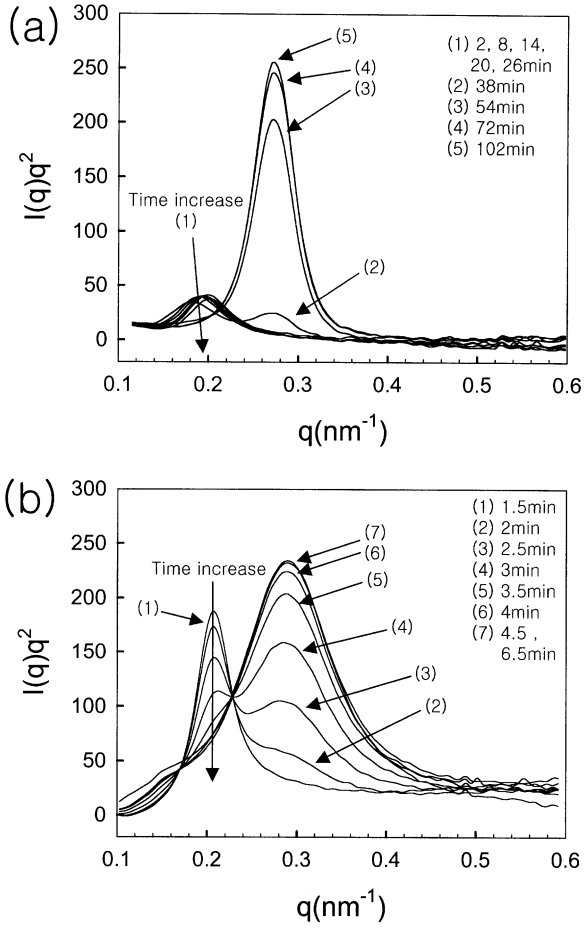

Fig. 16. Lorentz-corrected SAXS intensity versus q for PLLA-*b*-PCL(L) at various crystallization times at two temperatures: (a) 140°C; (b) 110°C.

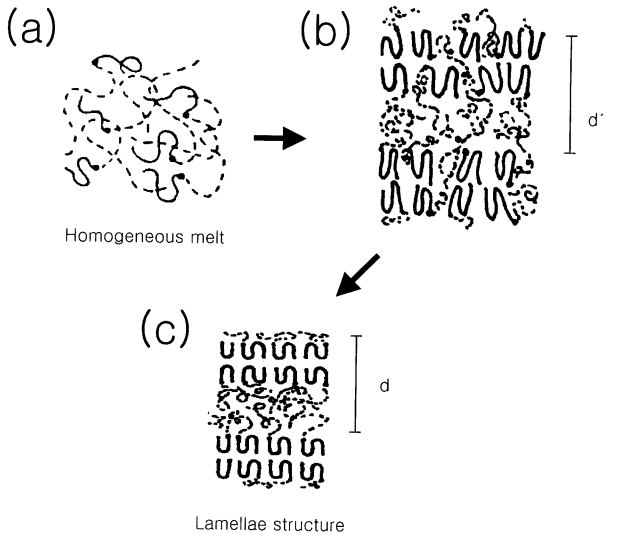

Fig. 17. The crystallization mechanism of the PLLA-*b*-PCL(L) with time.

It should be noted that the peak position near $q = 0.2\ \mathrm{nm}^{-1}$ in Fig. 16 was almost the same as the peak position of PLLA-*b*-PCL(L) at 170°C, as shown in Fig. 18. Note that these SAXS profiles were obtained during heating at a rate of 1°C/min after crystallized at 110°C for 2 h. The SAXS profiles between 110 and 145°C are almost the same in these plots.

It was seen that the peak position of q was shifted to a lower value with the increase of the crystallization temperature. This is because the lamellae thickness increases as the crystallization temperature approaches to T_m, as found at most crystalline polymers with flexible chains. Since we found that the crystallization peaks measured by WAXS were not observed at 170°C [39], the q^* at $0.2\ \mathrm{nm}^{-1}$ at 170°C does not correspond to the domain spacing between the PLLA crystalline part with a regular chain folding and the amorphous part. Thus, this $d\ (= 2\pi/q^*)$ might represent to the domain spacing similar to that given in Fig. 17(b). Interestingly, we found that the PLLA-*b*-PCL(H) exhibited a similar shift toward a lower q with increasing temperature, as shown in Fig. 19. However, a peak located at $0.1 < q < 0.2\ \mathrm{nm}^{-1}$ did not appear. The different behavior in SAXS profiles between PLLA-*b*-PCL(H) and PLLA-*b*-PCL(L) might be due to two reasons. First, the spacing corresponding to alternating lamellar layers, consisting of incomplete crystalline and amorphous regions, even if this exists, might be too large (e.g. $q < 0.1\ \mathrm{nm}^{-1}$); thus the SAXS does not detect it. Secondly, due to preexistence of the microdomain at molten state, the crystallization-induced microdomain is greatly suppressed. A further investigation is definitely needed to clarify the existence of the crystallization-induced microdomain formation.

From the plots of $\gamma(z)$ versus z for PLLA-*b*-PCL(L) at 140 and 110°C and complete crystallization, we found that L_c and d at 140°C were calculated to be 10.0 and 23.0 nm, respectively, while those at 110°C were 8.8 and 20.8 nm, respectively. The increase in L_c from 110 to 140°C for the PLLA-*b*-PCL(L) was 1.2 nm, which is just half of the increase in d (2.2 nm). Also, the values of L_c for PLLA-*b*-PCL(L) at 140 and 110°C are close to those for neat PLLA. These results led us to consider that the lamellar orientation of crystalline PLLA in PLLA-*b*-PCL(L) at two temperatures would be perpendicular orientations. This is also consistent with reports that when PE–PEE, PE–PEP, and PE–PVCH block copolymers with weak segregation or homogenous state in molten state are crystallized, the most probable lamellar orientations are perpendicular [7,11,23].

Before closing this part, we consider once more the chain folding of two PLLA-*b*-PCLs. The L_c of the PLLA-*b*-PCL(H) at each crystallization temperature is even smaller than that of PLLA-*b*-PCL(L) even though the larger molecular weights of the PLLA block. If PLLA block in both copolymers has the same chain folding (such as

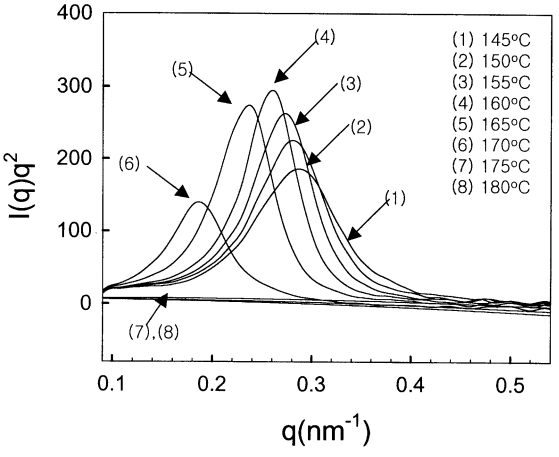

Fig. 18. Lorentz-corrected SAXS intensity versus q for PLLA-*b*-PCL(L) at various temperatures. The specimen was crystallized at 110°C for 2 h, and the SAXS profiles were measured during heating at a rate of 1°C/min.

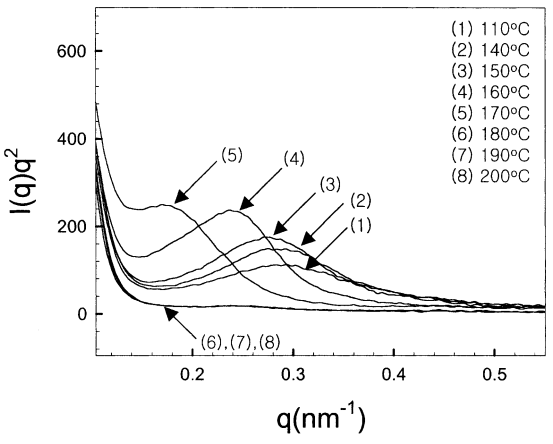

Fig. 19. Lorentz-corrected SAXS intensity versus q for PLLA-*b*-PCL(H) at various temperatures. The specimen was crystallized at 110°C for 2 h, and the SAXS profiles were measured during heating at a rate of 1°C/min.

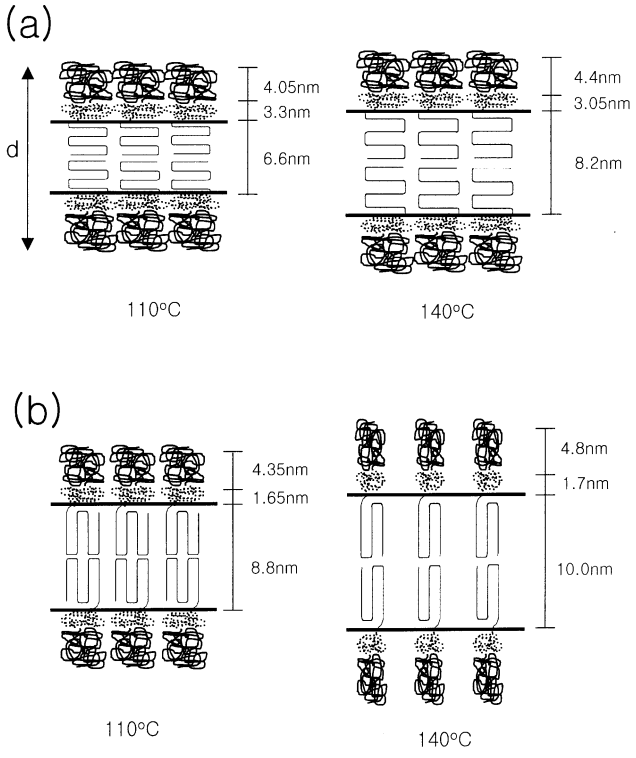

Fig. 20. A schematic of the chain folding as well as the domain spacing of the amorphous PCL block (the upper), the amorphous PLLA block (middle), and the crystalline PLLA block (the lower) for (a) PLLA-*b*-PCL(H) and (b) the PLLA-*b*-PCL(L) at 110 and 140°C.

perpendicular folding), one theory [41] suggests that the d is proportional to $N_{total}N_a^{-5/12}$ where N_{total} is the total number of segments (or degree of polymerization) of a block copolymer and N_a is the number of segments of the amorphous block (PCL block). The predicted d of the PLLA-*b*-PCL(H) was 2.4 times larger than that of the PLLA-*b*-PCL(L). This is far from the experimental results (~1). On the other hand, the d of the PLLA-*b*-PCL(M) at 110 and 140°C were 37 and 32 nm, respectively [39]. These values are 1.54–1.61 times those of the PLLA-*b*-PCL(L), which is very close to the prediction (1.49). These results suggest that the chain folding in the PLLA-*b*-PCL(L) was very similar to that in the PLLA-*b*-PCL(M), but quite different from that in the PLLA-*b*-PCL(H). On the basis of these results, we can draw a schematic of the chain folding as well as the domain spacing for two block copolymers at two temperatures, as shown in Fig. 20. Here, the amorphous PCL block spacing ($L_{a,PCL}$) located at the uppermost part was calculated by the total spacing (d) multiplied by volume fraction. The amorphous PLLA spacing ($L_{a,PLLA}$) was simply determined by $d - L_{a,PCL} - L_c$. We found that the crystallinity of the PLLA block calculated from $L_{a,PLLA}/(L_c + L_{a,PLLA})$ on the basis of Fig. 20 is comparable to those obtained from WAXS results.

4. Conclusion

In this study, we synthesized PLLA-*b*-PCL by using a macroinitiator of PCL-OH. The PLLA-*b*-PCL(H) showed microphase-separated structures at molten state up to 220°C, as determined from rheological measurement, while PLLA-*b*-PCL(L) became homogeneous at temperatures higher than the T_m of PLLA.

From the DSC and OM images, the crystallization mechanism of the PLLA-*b*-PCL(H) might be different from that of the PLLA-*b*-PCL(H). From the SAXS and WAXS experiments at 110 and 140°C, we concluded that the chain folding of crystalline PLLA of PLLA-*b*-PCL(H) at two temperatures was parallel orientations, while that of PLLA-*b*-PCL(L) was perpendicular. These results suggest that the chain segregation between the blocks at molten state affected significantly the chain folding of a block copolymer during the crystallization. For earlier crystallization times, PLLA-*b*-PCL(L) becomes microdomain structure having an incomplete crystalline part of PLLA block and amorphous PCL block. This domain spacing was larger than the domain spacing of the crystalline part of PLLA block with complete lamellar ordering and the amorphous part.

Acknowledgements

I acknowledge for the helpful discussions with Profs. S. Nojima at JAIST and S. Sakurai at Kyoto Institute of Technology. This work was supported by KOSEF (97-05-02-03-01-3), a special POSTECH Research Instrument grant (1999), and Applied Research Center (2000 G0202). Synchrotron SAXS experiments were performed at the PLS (1B2 and 3C2 beam lines) in Korea, which was supported by MOST and POSCO.

References

[1] Vainionpaa S, Pentti Rokkanen P, Tormala P. Prog Polym Sci 1989;14:679.
[2] Ohtaki A, Sato N, Nakasaki K. Polym Degr Stab 1998;61:499.
[3] Mohajer Y, Wilkes GL, Wang IC, McGrath JE. Polymer 1982;23:1523.
[4] Seguela R, Prud'homme J. Polymer 1989;30:1446.
[5] Cohen RE, Cheng PL, Douzinas K, Kofinas P, Berney CV. Macromolecules 1990;23:324.
[6] Douzinas KC, Cohen RE. Macromolecules 1992;25:5030.
[7] Cohen RE, Bellare A, Drzewinski MA. Macromolecules 1994;27:2321.
[8] Rangarajan P, Register RA, Fetters LJ. Macromolecules 1993;26:4640.
[9] Rangarajan P, Register RA, Fetters LJ, Bras W, Naylor S, Ryan AJ. Macromolecules 1995;28:4932.
[10] Rangarajan P, Register RA, Adamson DH, Fetters LJ, Bras W, Naylor S, Ryan AJ. Macromolecules 1995;28:1442.
[11] Ryan AJ, Hamley IW, Bras W, Bates F. Macromolecules 1995;28:3860.
[12] Hamley IW, Fairclough JPA, Bates FS, Ryan AJ. Polymer 1998;39:1429.

[13] Quiram DJ, Register RA, Marchand GR. Macromolecules 1997;30:4551.
[14] Hamley IW, Fairclough JPA, Terrill NJ, Ryan AJ, Lipic PM, Bates FS, Towns-Andrews E. Macromolecules 1996;29:8835.
[15] Hamley IW, Fairclough JPA, Ryan AJ, Bates FS, Towns-Andrews E. Polymer 1996;37:4425.
[16] Ashman PC, Booth C. Polymer 1975;16:889.
[17] Booth C, Dodgson DV. J Polym Sci: Polym Phys Ed 1973;11:265.
[18] Mai SM, Fairclough JPA, Viras K, Gorry PA, Hamley IW, Ryan AJ, Booth C. Macromolecules 1997;30:8392.
[19] Ryan AJ, Fairclough JPA, Hamley IW, Mai SM, Booth C. Macromolecules 1997;30:1723.
[20] Nojima S, Kato K, Yamamoto S, Ashida T. Macromolecules 1992;25:2237.
[21] Nojima S, Ono M, Ashida T. Polymer J 1992;24:1271.
[22] Nojima S, Yamamoto S, Ashida T. Polymer J 1995;27:673.
[23] Hamley IW. The physics of block copolymers. New York: Oxford University Press, 1998. Chapter 5.
[24] Int'Veld PJA, Velner EM, Van De Witte P, Hamhuis J, Dijkstra PJ, Feijen J. J Polym Sci: Polym Chem Ed. 1997;35:219.
[25] Bero M, Kasperczyk J. Macromol Chem Phys. 1996;197:3251.
[26] Park BJ, Rah SY, Park YJ, Lee KB. Rev Sci Instrum 1995;66:1722.
[27] Han CD, Kim J, Kim JK. Macromolecules 1989;22:383.
[28] Han CD, Baek DM, Kim JK. Macromolecules 1990;23:561.
[29] Han CD, Kim JK. Polymer 1993;34:2533.
[30] Han CD, Baek DM, Kim JK, Ogawa T, Sakamoto N, Hashimoto T. Macromolecules 1995;28:5043.
[31] Kim JK, Lee HH, Sakurai S, Aida S, Masamoto J, Nomura S, Kitagawa Y, Suda Y. Macromolecules 1999;32:6707.
[32] Mark JE, editor. Polymer data handbook. New York: Oxford University Press, 1999. p. 628.
[33] Crescenzi V, Manzini G, Calzolari G, Borri C. Eur Polym 1972;8: 449.
[34] Fischer EW, Sterzel HJ, Wegner G, Kolloid Z. Z Polym 1973;251:980.
[35] Kobayashi J, Asahi T, Ichiki M, Okikawa A, Suzuki H, Watanabe T, Fukuda E, Shikinami Y. J Appl Phys 1995;77:2957.
[36] Hsiao BS, Gardner KH, Wu DQ, Chu B. Polymer 1993;34:3986.
[37] Stroble G. The Physics of polymers. New York: Springer, 1996. Chapter 4.
[38] Chen HL, Liu HH, Lin JS. Macromolecules 2000;33:4856.
[39] Kim JK, Lee MS, Unpublished results (2000).
[40] Bates FS, Fredrickson GH. Annu Rev Phys Chem 1990;41:525.
[41] Whitmore MD, Noolandi J. Macromolecules 1988;21:1482.